



## Article

<https://doi.org/10.1038/s41561-025-01704-5>

# Non-collisional orogeny in northeast Japan driven by nearby same-dip double subduction

Received: 8 August 2024

Guido M. Gianni<sup>1,2</sup>✉, Zonglin Guo<sup>3</sup>, Adam F. Holt<sup>3</sup> & Claudio Faccenna<sup>1,4</sup>

Accepted: 16 April 2025

Published online: 05 June 2025

Check for updates

Same-dip double subduction systems influence plate kinematics, geometry and mantle flow within the region bounded by the two subduction zones. However, whether these effects extend to nearby plate margin tectonics remains an open question. Furthermore, the range of geodynamic processes operating in these margins and driving non-collisional orogeny (that is, the formation of Andean-type mountain ranges) is not yet fully understood. Here we explore the potential geodynamic connection between the tectonic evolution of northeast Japan and the development of the Ryukyu/Izu–Bonin–Marianas same-dip double subduction using three-dimensional geodynamic models. We find that this same-dip double subduction drags the Pacific trench westwards, resulting in northward-propagating trench advance and compression affecting the northeastern Japan arc and back-arc. We thus propose that the dynamics of the Ryukyu/Izu–Bonin–Marianas same-dip double subduction over the past ~10–5 Myr drove the enigmatic plate kinematics responsible for non-collisional orogeny and back-arc subduction initiation in northeast Japan since ~6–3.5 Myr ago, which has made this region prone to catastrophic earthquakes. We also suggest that same-dip double subduction explains various ancient episodes of widespread non-collisional orogenesis and represents a mechanism through which subduction zones establish the plate kinematic conditions necessary for non-collisional orogenesis.

Subduction zones are critical features of our planet, providing the forces needed to move tectonic plates and deform margins, develop volcanic arcs and sedimentary basins, and unleashing the most devastating megathrust earthquakes<sup>1</sup>. In recent years, researchers have observed that these geodynamic settings can be substantially altered by the emergence of a nearby subduction zone, usually forming so-called double subduction systems. These impacts include dramatic changes in plate kinematics, trench motions, slab dips and the associated mantle flow<sup>2–9</sup>.

Double subduction zones occur in three discernible geometries: divergent double subduction<sup>10</sup>, evident in active settings such as the

Molucca Sea subduction zones<sup>9</sup> and the Mediterranean region<sup>4</sup>; convergent double subduction, typified by areas hosting oppositely dipping subduction zones, such as those surrounding the Caribbean plate<sup>11</sup> and Southeast Asia<sup>12</sup>; and same-dip double subduction (SDDS), which features both ancient and active examples like the Mesozoic Neoethyan arc system<sup>3,6</sup> and the late Cenozoic Ryukyu/Izu–Bonin–Marianas SDDS<sup>2,5,13</sup> (Fig. 1a). Notably, recent investigations have highlighted the geodynamic impact of SDDS initiation, elucidating its role in driving major changes in direction and/or plate velocity<sup>3,6,14</sup>. Studies focused on the Ryukyu/Izu–Bonin–Marianas SDDS, involving the subduction

<sup>1</sup>German Research Centre for Geosciences (GFZ), Potsdam, Germany. <sup>2</sup>National Scientific and Technical Research Council (CONICET), Buenos Aires, Argentina. <sup>3</sup>Rosenstiel School of Marine, Atmospheric, and Earth Science, University of Miami, Miami, FL, USA. <sup>4</sup>Dipartimento di Scienze, Università degli Studi Roma Tre, Rome, Italy. ✉e-mail: [guidogianni22@gmail.com](mailto:guidogianni22@gmail.com)

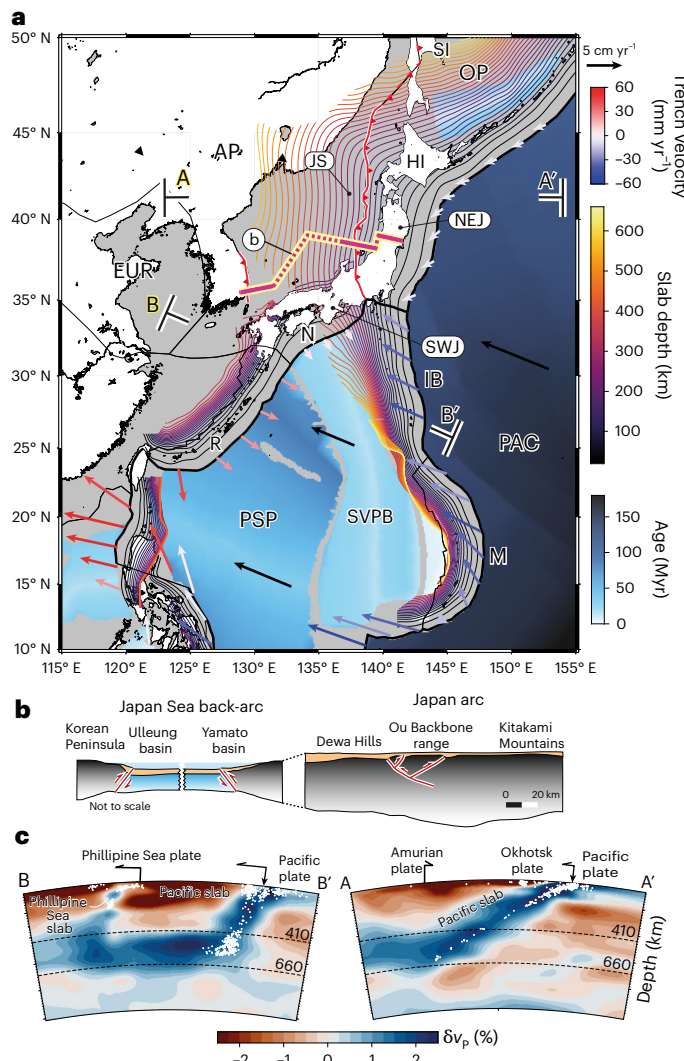


**Fig. 1 | Present-day plate kinematic setting and mantle structure of the western Pacific subduction zone.** **a**, Map indicating the major tectonic plates in the study area, subduction isodepths<sup>57</sup>, absolute trench and upper plate kinematics<sup>40</sup>, the location of northeast Japan and the Japan Sea, and the Ryukyu–Nankai/Izu–Bonin–Marianas SDDS system. Negative and positive trench velocity values corresponds to trench advance and retreat, respectively. **b**, A composite structural cross-section from the northeast Japan arc<sup>29</sup> to the back-arc region up to the eastern Korean margin<sup>28</sup> (location shown in **a**). **c** Seismic tomography sections<sup>39</sup> showing the mantle structure and slab seismicity associated with the northeastern Japan subduction and the Ryukyu/Izu–Bonin–Marianas SDDS system. EUR, Eurasian plate; AP, Amurian plate; PSP, Philippine Sea plate; PAC, Pacific plate; OP, Okhotsk plate; HI, Hokkaido Island; SI, Sakhalin Island; NEJ, northeastern Japan; SW, southwest Japan; JS, Japan Sea; R, Ryukyu trench; N, Nankai trench; IB, Izu–Bonin subduction segment; M, Marianas subduction segment; SVPB, extinct Shikoku–Parece–Vela back-arc basin; δVp (%), percent perturbation (or deviation) of P-wave velocity relative to a reference Earth model.

of the Pacific plate beneath the Philippine Sea plate, which in turn subducts beneath the Eurasian plate along the Ryukyu–Nankai trench, indicate that this system leads to Pacific slab steepening and trench advance<sup>2,5,13,15</sup> (Fig. 1a–c). Taken together, these findings suggest that the geodynamics of many subduction zones is best understood when considering these plate boundaries as components within larger-scale subduction networks. This opens up exciting avenues for understanding active margin dynamics and, more specifically, the magnitudes and length scales at which double subduction is relevant. In this regard, while most studies on SDDS have focused on the effects confined to

the area of double plate convergence, the broader influence of SDDS on nearby plate margin tectonics remains unknown.

Here we assess this issue by analysing the geological evolution of northeast Japan and the neighbouring Ryukyu/Izu–Bonin–Marianas SDDS, presenting evidence for what we define as double subduction-induced orogeny. We hypothesize that the initiation of the Ryukyu/Izu–Bonin–Marianas SDDS modifies trench kinematics along the Pacific subduction, triggering non-collisional compression in northeast Japan and inducing the active subduction initiation process in the eastern Japan Sea. We test this hypothesis through geologically constrained three-dimensional (3D) geodynamic numerical experiments on double subduction, illustrating how SDDS impacts tectonic stress within the overriding plates of adjacent active margins. The tectonic consequences of SDDS onset illustrate a mechanism whereby complex plate tectonic interactions create optimal plate kinematic conditions for non-collisional orogeny<sup>16</sup>.

## Late Cenozoic tectonic evolution of northeast Japan

During the Oligocene–Miocene epoch (~25–20 Myr ago; Ma), several marginal basins, including the Japan Sea back-arc basin, and the Shikoku and Parece–Vela basins of the Philippine Sea plate, underwent simultaneous opening caused by the eastward Pacific trench retreat and major strike slip tectonics<sup>17–20</sup> (Figs. 1a and 2a,b). This process caused the Japanese Island arc to separate from the Asian continental margin through accelerated back-arc rifting during the early to middle Miocene<sup>17,20–22</sup>. This culminated ~16–15 Ma, resulting in the formation of a 3–3.7-km-deep basin with rifted continental crust and local oceanic floor (for example, refs. 17,18,23,24; Figs. 1a and 2b). In northeast Japan, neutral stress conditions during thermal subsidence progressively changed from mild east–west compression since ~10–8 Ma to highly compressional since ~5.6–3.5 Ma<sup>17–20,25,26</sup> (Fig. 2b). Pliocene–Quaternary east–west compression led to 10–15 km of shortening within northeast Japan<sup>25</sup>, propagating westwards to the Japan Sea<sup>25,27</sup> and the east Korean margin<sup>28</sup>. Currently, the shortening is distributed across several east- and west-dipping thrusts and basin inversion structures<sup>19,20,25–27,29</sup>, with rates reaching up to 15 mm yr<sup>-1</sup> off central Japan<sup>30</sup> (Fig. 1b). A compilation map of active faulting shows that compression affects a ~1,200-km-long deformed belt extending into the back-arc region west of Hokkaido Island (see Fig. 5 in ref. 20). The structural observations, coupled with the documentation of thrust earthquakes occurring in this area over the past century, with magnitudes ranging from  $M_w$  6.9 to 7.8, have prompted several authors to propose incipient subduction initiation in the eastern Japan Sea (for example, refs. 27,31,32; Fig. 1a,b). Active back-arc faulting in this region was responsible for the recent Noto Hanto earthquake (2024,  $M_w$  7.6) that generated strong ground motion, large crustal deformation and tsunamis that caused major damage in the region<sup>33</sup>. Recent studies also reported geological and geophysical evidence for diffuse subduction initiation along the eastern Korean margin active since ~5 Ma<sup>28</sup> (Fig. 1a,b). To the south, tectonics are locally dominated by the interaction of the Izu–Bonin arc (Fig. 1a). This area is characterized by a main phase of arc subduction and deformation occurring since ~6–5 Ma and crustal motion within the active fault system controlled by the indented configuration of the plate boundary (for example, refs. 20,34).

## Hypotheses for the origin of northeast Japan compression

The origin of the Pliocene–Quaternary compressional tectonic regime across the northeastern Japanese active margin and the back-arc Japan Sea remains highly contentious. One hypothesis suggests a predominant role for the lower plate<sup>35</sup>, proposing that the Pacific plate accelerated since ~5 Ma, introducing a significant compression component normal to the Japan trench<sup>36</sup>. However, in this mechanism, it is unclear why compression localized only in northeast Japan and not along the entire high-convergence western Pacific subduction<sup>37</sup>. Moreover, in

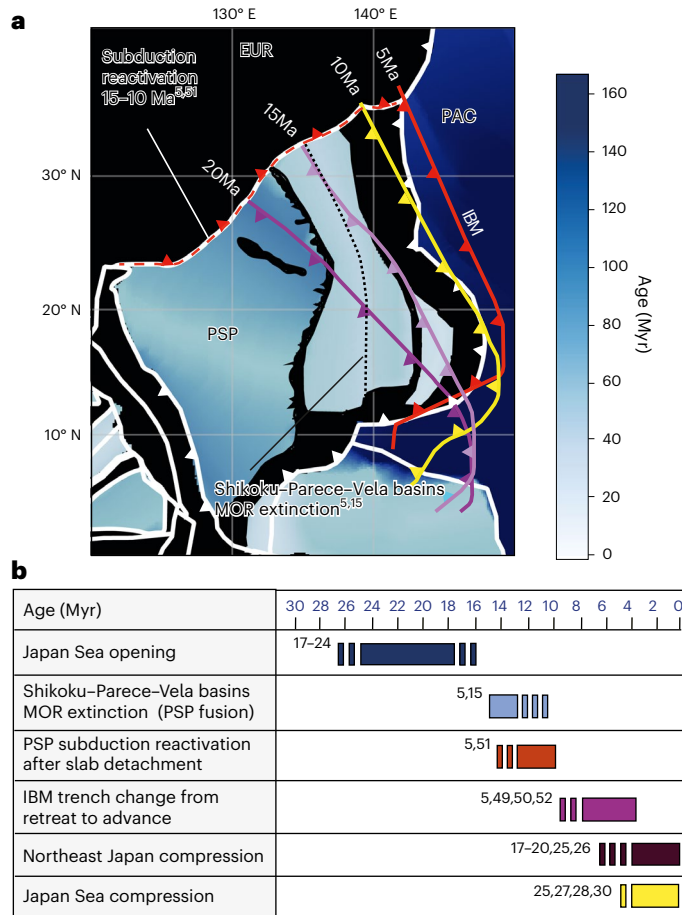


**Fig. 2 | Cenozoic kinematics of the Izu–Bonin–Marianas trench and its relationship to deformation events in the arc and back-arc regions of northeast Japan.** **a**, Evolution of the Izu–Bonin–Marianas trench migration in the late Cenozoic from ref. 5 that considers a moving Indian/Atlantic hotspot reference frame<sup>41</sup>. **b**, Time correlation of tectonic and kinematic changes in the study area. Note that the progressive shift in the motion of the Izu–Bonin–Marianas trench, following Philippine Sea plate fusion and the reactivation of subduction along the Ryukyu–Nankai trench, slightly precedes and overlaps with the onset of strong compressional conditions in northeast Japan and the Japan Sea back-arc basin. IBM, Izu–Bonin–Marianas trench; EUR, Eurasian plate; PSP, Philippine Sea plate; PAC, Pacific plate; MOR, mid-ocean ridge. Panel **a** reproduced with permission from ref. 5, Elsevier.

global surveys of all major subduction zones, high plate convergence does not correlate with upper plate compression<sup>38</sup>. An alternative, classic hypothesis highlights the impact of eastward upper plate motion, which is attributed to the clockwise rotation of the Amurian plate in response to the distant effects of the India–Eurasia collision<sup>19,22,27</sup>. This rotation would have triggered slow convergence between the Amurian plate and the Okhotsk plate along the eastern margin of the Japan Sea. Nevertheless, Amurian plate extrusion has been an ongoing process since at least the late Oligocene–early Miocene<sup>39</sup>, complicating a direct link with the Pliocene onset of compression in northeast Japan and its back-arc region. Furthermore, while the motion of the upper plate towards the trench is significant, it alone does not suffice to initiate compression because upper plate deformation is driven by the relative difference between upper plate and trench motion<sup>16</sup>. It is therefore crucial to examine how the movement of the upper plate interacts with trench dynamics to fully understand the triggering of compression.

Both global parametric analyses and simple conceptual/kinematic models indicate that plate margin compression is favoured when the trench retreat velocity is less than the upper plate velocity<sup>37</sup>. In the study

area, the Japan trench east of northeast Japan is advancing at rates of 0.7–0.6 cm yr<sup>-1</sup> in a seafloor-spreading aligned absolute reference frame<sup>40</sup>, resulting in an overall convergence with the near-stationary upper plate (in the same reference frame), and thus meeting the plate kinematic conditions for upper plate compression (Fig. 1a). These kinematic conditions are still met even when analysing other widely used absolute plate motion reference frames<sup>41–43</sup>. Based on this, it has been suggested that the presence of a wide Pacific slab, preventing rapid slab rollback and trench retreat combined with a trenchward-moving upper plate, created this plate kinematic condition in northeast Japan<sup>37</sup> (Fig. 1a,b). However, this conflicts with robust plate reconstructions including mantle slab records suggesting the subduction of a wide Pacific plate since 50–40 Ma (for example, ref. 44), well before the onset of regional compression in the study area. The Pacific kinematic conditions driving compression in the study area have also been associated with the clockwise rotation and northwestward movement of the Philippine Sea plate<sup>45</sup>. However, major rotation of this plate occurred since at least ~30–40 Ma<sup>44,46</sup>, again significantly before the onset of compression in northeast Japan (Fig. 2a,b).

Alternatively, recent numerical experiments on Pacific subduction<sup>47</sup> suggest that the plate kinematics leading to compression may result from a combination of an imposed eastward asthenospheric flow and slab folding processes at depth, resulting in several trench retreat–advance cycles since 50 Ma. The issue with the applicability of this model to northeast Japan is that these experiments predict an extensional phase from 6 to 3 Ma, whereas geological data indicate strong and continuous compression since then<sup>17–20,25,26</sup> (Fig. 2b). Moreover, the many alternations of compression and extension since ~35 Ma, as shown in their modelling results, do not correlate well with geological data and the overall tectonic evolution of this specific region (see previous section; Fig. 2b).

Lastly, alternatives such as compression triggered by subduction or accretion of bathymetric highs are unlikely due to the localized nature of the associated compression<sup>37,38</sup>. More importantly, the absence of a major aseismic ridge or oceanic plateaus interacting with the northeastern Japan trench—features necessary to induce eastward-directed compression—further diminishes the plausibility of this hypothesis. The only bathymetric high that may influence compression is the Izu–Bonin arc (Fig. 1a). However, as previously shown<sup>34</sup>, it is considered more of a local factor, with its main deformational effects not extending more than approximately 150–200 km north of the accretion zone. Therefore, it cannot account for the documented ~1,200-km-long region under compression, as evidenced by both active and ancient thrust faults, as well as thrust-related intraplate earthquakes observed over the past few decades (see Fig. 5 in ref. 20).

In summary, over the past ~5–6 Ma, the northeast Japan arc-to-back-arc region has experienced increasing compression due to the onset of a plate kinematic context associated with an advancing trench. Existing explanations for this phenomenon are either unfeasible<sup>35,36,47</sup> or appear incomplete<sup>19,22,27,37,38,45</sup>. More importantly, numerical geodynamic models specifically designed to test conceptual frameworks in this region are still lacking.

## Double subduction-induced orogeny in northeast Japan

To investigate the geodynamic mechanisms driving effective plate kinematic conditions for non-collisional orogeny in northeast Japan over the past ~5.6–3 Myr, it is essential to consider trench kinematics and the Cenozoic evolution of Pacific subduction. Present-day trench kinematics<sup>40</sup>, spanning from northeast Japan to the Izu–Bonin–Marianas subduction segments (that is, Pacific trench in this study), depict a southward increase in westward trench advance (Fig. 1a). This southward shift in trench motion, towards increased advance, is also observed in various trench motion catalogues and is independent of the chosen absolute reference frame<sup>41–43,48</sup>. A potential explanation for

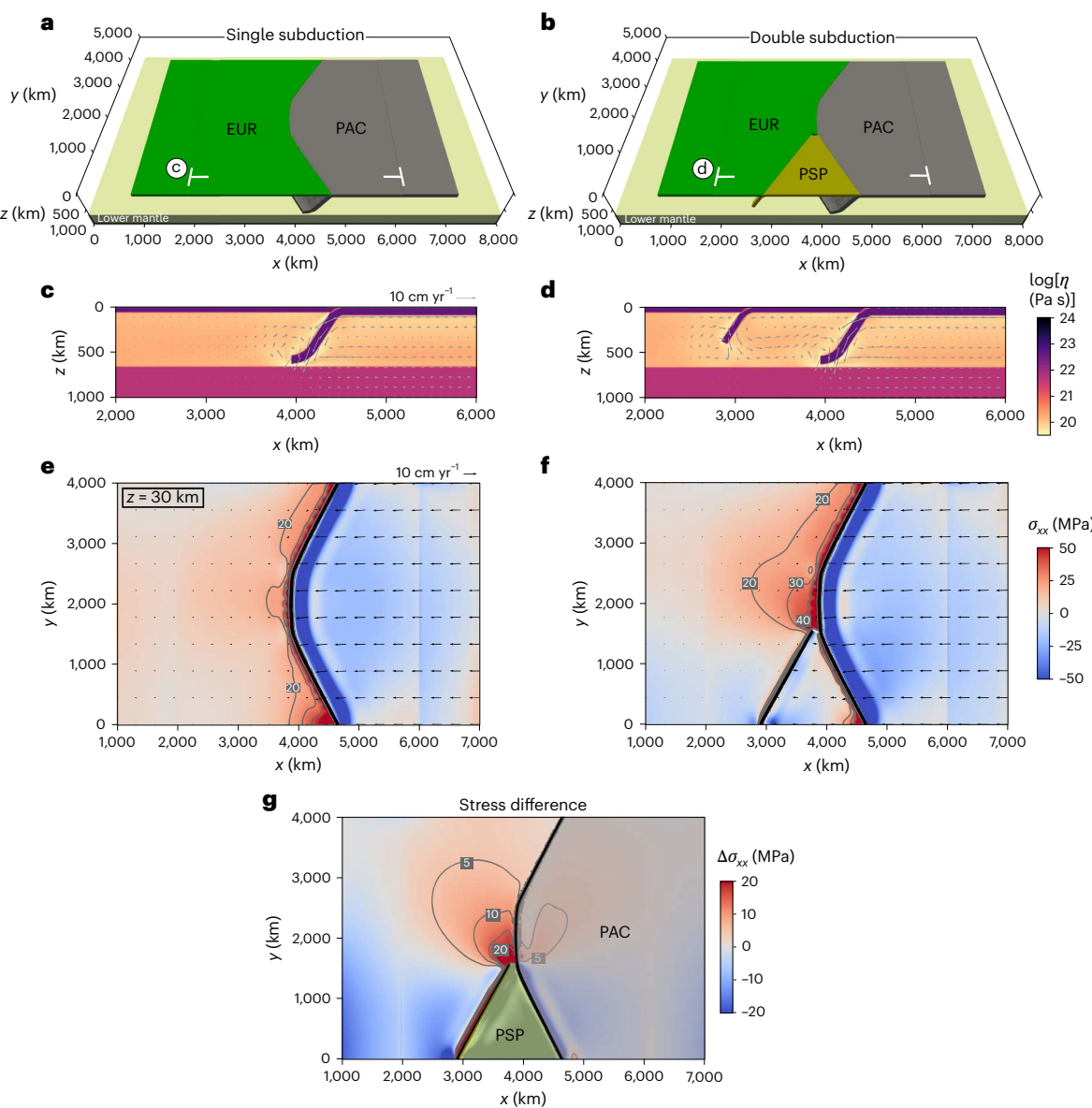


**Fig. 3 | Three-dimensional numerical subduction models testing the influence of the Ryukyu/Izu–Bonin–Marianas SDDS on driving upper plate compression in the northeastern arc-to-back-arc regions of Japan. a–f.** Set up for single (a) and double (b) subduction experiments, with the viscosity and velocity fields in cross-sections (c,d) and the computed trench-perpendicular (x-direction) normal stress field ( $\sigma_{xx}$ ) and plate velocity (e,f) for the reference

single and double subduction models, respectively. Stress and velocity are extracted within the lithospheric plates at 30 km depth. g, The normal stress difference between the models indicating significantly enhanced compression in the area corresponding to the location of northeast Japan. For simplicity, the Okhotsk plate is not included, and only an equivalent to the Eurasian plate is considered. EUR, Eurasian plate; PSP, Philippine Sea plate; PAC, Pacific plate.

the induced compression in Japan is then that forces associated with this Izu–Bonin–Marianas trench advance are transmitted northwards to this region. In this scenario, the slowly moving upper plate resists the west-directed force associated with trench advance, as transmitted from the south, and that this results in compression in the northeastern Japan arc and back-arc region (Fig. 1a,b). If this is correct, we would expect a temporal correlation between the initiation of trench advance in the Izu–Bonin–Marianas subduction zone and compression in northeastern Japan and the Japan Sea.

The onset of trench advance along the Izu–Bonin–Marianas subduction zone has been linked to a reorganization of major tectonic boundaries associated with the evolution of the Ryukyu/Izu–Bonin–Marianas SDDS<sup>2,5,13,15</sup>. Between ~40 and 15 Ma, the Izu–Bonin–Marianas trench predominantly underwent rapid, intermittent retreat<sup>17–20</sup>, shifting progressively to trench advance since ~10–5 Ma<sup>2,5,13,15,49,50</sup> (Fig. 2a,b).

Numerical models support the hypothesis that subduction reactivation of the Philippine Sea plate since 15–10 Ma in the Ryukyu–Nankai trench, following a slab detachment caused by ridge subduction<sup>5,51</sup>, exerted a pronounced northwestward pull on the Philippine Sea plate, consequently driving Pacific trench advance and facilitating the steepening of the Pacific slab (Fig. 2a). Recent numerical studies indicate that the initial stage of Ryukyu subduction (~30–15 Ma) did not significantly affect the Izu–Bonin–Marianas trench motion, most probably due to ineffective stress transmission caused by a thermally weakened upper plate at the Shikoku–Parece–Vela basins back-arc spreading centre<sup>15</sup>. However, after this system cooled and strengthened/fused since ~15–10 Ma, the reactivated Ryukyu subduction exerted a strong pull, driving the trench advance observed today<sup>5,52</sup> (Fig. 2b).

We note that the progressive shift in trench motion for the Izu–Bonin–Marianas trench since ~10–5 Ma<sup>5,49,50,52</sup> slightly precedes and

coincides with the onset of strong compressional conditions in northeast Japan and the Japan Sea back-arc basin since ~5.6–3 Ma<sup>17–20,25–28,32</sup> (Fig. 2b). These observations indicate a potential causal relationship between the reactivation of the Ryukyu/Izu–Bonin–Marianas SDDS after Philippine Sea plate fusion/strengthening, trench advance, and the onset of the compressional regime in northeast Japan and the incipient subduction in the Japan Sea.

## Geodynamic models of double subduction-induced orogeny

To evaluate the viability of double subduction-induced orogeny in northeast Japan, we set up 3D numerical subduction models (Methods, Fig. 3a–g and Extended Data Figs. 1–6). Our aim was to examine whether the insertion of an additional (Ryukyu–Nankai) subduction zone enhances compression within the northeast Japan upper plate region relative to a single subduction model containing only Pacific plate subduction along the Japan–Izu–Bonin–Mariana trenches. We therefore modelled two subduction scenarios—with and without subduction along the Ryukyu–Nankai trench (that is, single versus double subduction)—using the Advanced Solver for Planetary Evolution, Convection and Tectonics (ASPECT) finite element code<sup>53–56</sup> (Fig. 3a,b).

In our models, we solve for the velocity and stress fields associated with imposed slab and tectonic plate geometries. The plan-view margin shapes are an idealized representation of the present-day plate geometry. The Pacific and Philippine Sea subduction geometries are based on the present-day slabs, as delineated by earthquake hypocentres and seismic tomography<sup>57–59</sup> (Fig. 1c). We do not model the transition from single to double subduction; rather, we intend to represent the change in stress state from before (~10 Ma) to significantly after Ryukyu–Nankai subduction reinitiation<sup>5,51</sup> (present day). We therefore run our ‘pseudo-instantaneous’ single and double subduction models for only 10 kyr; this is sufficiently short that the plate and slab geometry undergoes minimal evolution from the geometries imposed. In both models, we considered a single, mechanically continuous (that is, no weak back-arc area<sup>15</sup>) upper plate, and identical Pacific plate/slab geometries. We adopt a linear viscous rheology for the lithosphere and crust, and we use a simplified power-law viscous rheology for the underlying flowing mantle. This enables us to hone in on the as yet unexplored first-order impact of double subduction on the upper plate stress state, while avoiding complexities associated with a large number of rheological parameters. Here we focus on two models (single and double subduction) with equivalent crustal viscosities ( $\eta_{\text{crust}} = 5 \times 10^{19} \text{ Pa s}$ ) and lithospheric strengths relative to the underlying mantle ( $\eta_{\text{lith}}/\eta_{\text{mantle}} = 500$ ). We chose the viscosity values to be intermediate within the ranges inferred from various geophysical, geodynamic and experimental constraints (for example, refs. 60–65), and to produce tectonic plate velocities compatible with those observed in the western Pacific, but we have also run additional tests to verify our first-order conclusions are unchanged if we vary these values (Extended Data Figs. 1 and 2).

In the single subduction model, the Pacific trench advances slowly to the left/west at ~2 cm yr<sup>-1</sup> and far-field Eurasia is near-stationary (Fig. 3e and Extended Data Fig. 3). Pacific plate motion is trench-perpendicular and at ~8–10 cm yr<sup>-1</sup> with respect to far-field Eurasia. These modelled velocities exhibit first-order agreement with observed plate velocities in seafloor-spreading aligned<sup>40,48</sup> or fixed Pacific hotspot reference frames<sup>43</sup>. Adding the Ryukyu–Nankai subduction zone induces a westward Pacific trench advance of 3–4 cm yr<sup>-1</sup> adjacent to the Philippine Sea plate (that is, Izu–Bonin–Mariana; Fig. 3f and Extended Data Figs. 1 and 4). This is consistent with observed trench motions<sup>48</sup> and previous subduction modelling<sup>13,52,66</sup> (Fig. 1a). These agreements suggest that our models capture the relevant large-scale geodynamic processes and are, in turn, suitable for investigating changes in the large-scale lithospheric stress state induced by double subduction.

Our numerical models show that the establishment of a double subduction system influences notably the upper plate stress state in the Japan triple junction and immediately north of this region (Fig. 3e–g and Extended Data Figs. 4 and 5). Without double subduction, the lithosphere in the Japan triple junction region is under relatively moderate trench-perpendicular compression of ~10–20 MPa (Fig. 3e and Extended Data Fig. 4a). In such geodynamic models, this absolute upper plate stress state is largely controlled by the imposed upper plate size, thickness, density and strength (for example, refs. 67,68). Here, we therefore focus on the relative change in stress state induced by double subduction, as opposed to absolute stress values. Throughout the upper plate, double subduction induces a notable increase in the magnitude of trench-perpendicular compressive stress (Fig. 3f and Extended Data Fig. 4b). Approximately 350 km onboard of the modelled Japan trench, that is, in the vicinity of thrusting in northeast Japan, the average trench-perpendicular compressive normal stress in the lithosphere doubles from ~20 MPa to ~40 MPa (Fig. 3g and Extended Data Fig. 5). The other normal stress components (vertical and trench-parallel) are only minimally affected by double subduction (Extended Data Fig. 4). This increase in trench-perpendicular compression is due to the along-strike transmission of the Philippine Sea plate slab pull at the Pacific margin<sup>15,52</sup>, which causes the Pacific slab to indent into the Eurasian upper plate at the northeast Japan trench, thereby inducing enhanced upper plate compression. The region experiencing increases in horizontal compressive stress extends significantly, covering an area ~1,000–1,200 km northwards along the Pacific trench and an additional ~1,300–1,500 km inland (Fig. 3g). This observation aligns with geological and geophysical evidence of compression, not only within the Japan arc but also in the back-arc domain, which includes a deformed belt approximately ~1,200 km in length<sup>17–20,25–28,30–32</sup> (Figs. 3g and 1a). The model results also highlight subtle compression extending north of northeast Japan, consistent with structural geomorphological, seismological and GPS data, all of which indicate mild compression/transpression along Sakhalin Island<sup>18,69</sup> (Fig. 1a). The observation that the increased compressional lithospheric stress in the models does not extend beyond approximately ~1,500 km aligns with newly derived strain maps of eastern Eurasia, which indicate negligible active deformation west of the analysed area<sup>70</sup> (Figs. 3g and 1a).

Additional tests also demonstrate that, irrespective of the chosen crustal and lithospheric strengths, an increase in trench-perpendicular horizontal compressive stress is a robust feature in transitioning from single to double subduction (Extended Data Figs. 1 and 2). The magnitude of the increase in horizontal compression varies with these properties—increasing for higher lithosphere viscosity or lower crustal viscosity—but the single-to-double stress increase is always prevalent. Hence, these results support the double subduction-induced orogeny hypothesis and provide an integrative geodynamic framework that links the evolution of the Ryukyu/Izu–Bonin–Marianas SDDS system<sup>2,5,13</sup>, the motion of the Philippine Sea plate, the associated westward drag of the Pacific trench<sup>45,49,50</sup> and the onset of arc-back-arc compression in northeast Japan<sup>17–20,25–28,32</sup>. We suggest that this process accounts for the transition from soft to hard deformation during Izu arc subduction between 8 and 6 Ma<sup>20</sup>.

## Double subduction-induced orogeny in the geological record

Despite the substantial variability in scale and geometrical configuration inherent to highly dynamic double subduction systems, the documentation of active double subduction-induced orogeny in northeast Japan has major implications for the orogenic evolution of plate margins proximal to other ancient SDDS systems.

We propose that double subduction-induced orogeny, generalized in Fig. 4a, offers a plausible explanation for the widespread Cretaceous compression documented west of the contemporaneous Neotethys subduction system<sup>71,72</sup> (Fig. 4b). Here, a major change in absolute plate

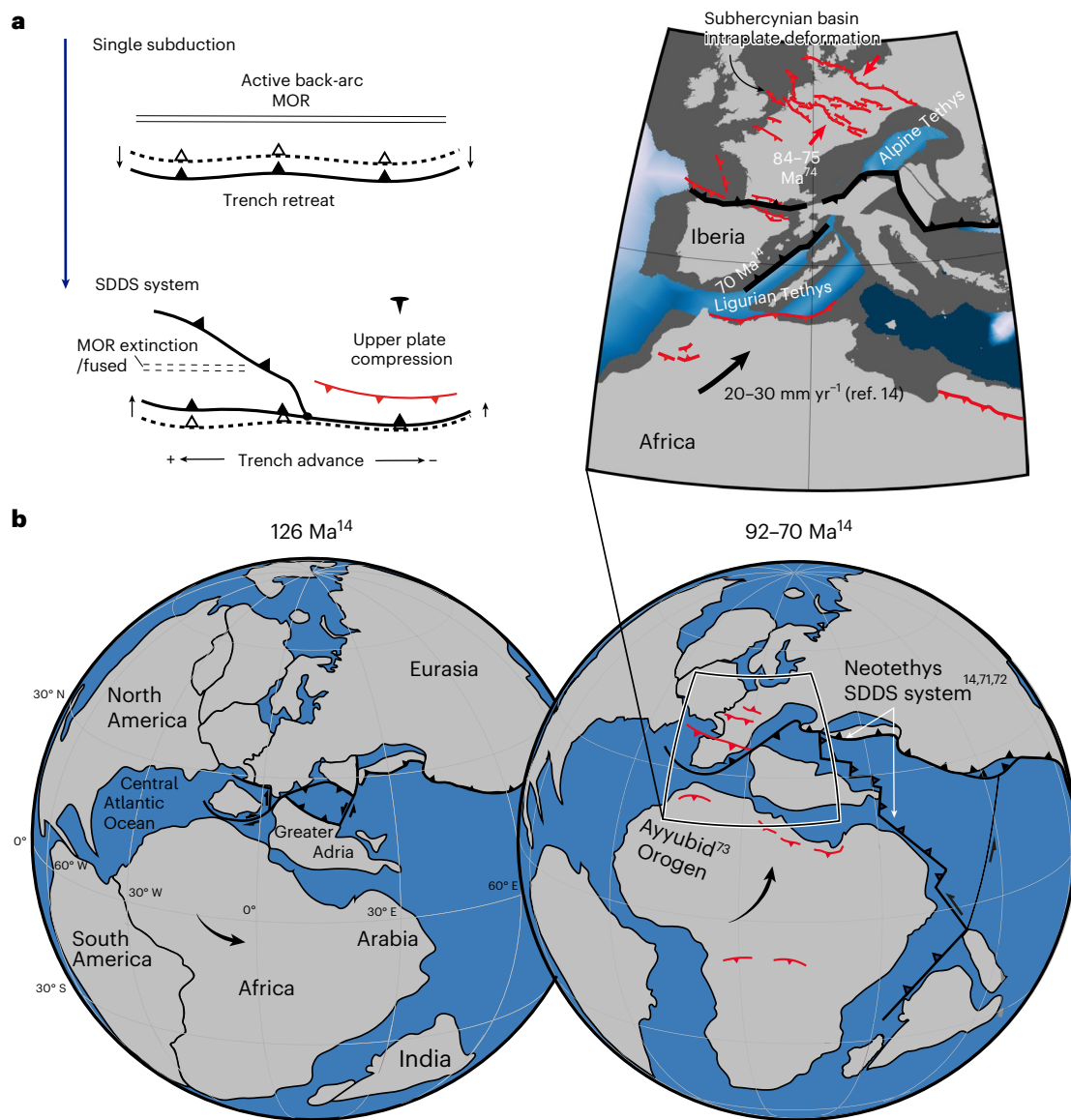


**Fig. 4 | Generalized conceptual model of double subduction-induced orogeny and a proposed Mesozoic case associated with the Neotethys SDDS system.** **a**, A conceptual model illustrating the impact on trench dynamics, transitioning from trench retreat to trench advance, triggered by the onset of an SDSS on a plate capable of transmitting slab pull between trenches. This model illustrates the tectonic effects of this process, highlighting plate margin compression occurring away from the SDSS. For simplicity, the upper-right panel depicts a fixed upper plate. The conceptual framework builds on the established

understanding of SDSS dynamics<sup>2,3,5,6,13–15</sup> and our own results on the tectonic effects on nearby plate margins. **b**, Proposal of a double subduction-induced orogenic event based on the documentation of Late Cretaceous plate margin and intraplate compression<sup>71,73,74</sup> west of the contemporaneous Neotethys SDSS system<sup>14</sup>. Global and regional plate kinematic reconstructions for the late Early to Late Cretaceous are from ref. 14 and ref. 39, respectively. Panel **b** adapted with permission from: main maps, ref. 14, Springer Nature Limited; inset, ref. 39 under a Creative Commons licence CC BY-NC-ND 4.0.

motion direction and the rapid northward drift of the African plate have been invoked to explain Late Cretaceous compression in northern Africa<sup>71</sup> (~86–84 Ma, Ayyubid Orogen<sup>73</sup>), subduction initiation along the western Mediterranean region<sup>14</sup> and far-field deformation in central Europe (~84–75 Ma, Subhercynian basin intraplate deformation<sup>74</sup>; Fig. 4b). Recent studies suggest that the onset of a ~12,000-km-long SDSS approximately 105 Ma<sup>72</sup>, along with the initiation of effective slab pull around ~95 Ma, coincided with the directional shift and acceleration in the drift of the African plate<sup>14</sup>. Updated plate kinematic data indicate that Africa–Eurasia relative plate motion along the western Mediterranean active margin transitioned from very slow motion (<5 mm yr<sup>-1</sup>) in a south–southeast direction between ~125 and 90 Ma to a northeast direction with a velocity of 30–20 mm yr<sup>-1</sup> from ~95 to 70 Ma<sup>14</sup> (Fig. 4b). Although differing in dimensions, exact configuration

and partially in the nature of the orogenic processes it involves—such as the collision of Iberia—we propose that, within the framework of the double subduction-induced orogeny concept introduced here (Fig. 4a), a potential genetic connection exists (Fig. 4b). Specifically, this connection links the lifespan (105–75 Ma) of the large neighbouring SDSS zone in the Neotethys Ocean with the associated plate kinematic change and the plate-wide compression (~90–75 Ma<sup>14,72</sup>) observed to the west of this system (Fig. 4b).

Although more speculative owing to the limited precision of early Palaeozoic plate margin reconstructions for southwest Gondwana, another potential candidate for ancient double subduction-induced orogeny is the Palaeozoic southern South American margin. Notably, the Chaitenia SDSS (~380–340 Ma) to the west of Patagonia<sup>75</sup> partially overlaps in time with the Chaní orogeny (~385–350 Ma) immediately

to the north of this ancient SDDS<sup>76</sup>. If active subduction characterized the entire margin at this time, as recently suggested<sup>77</sup>, and there was a north–south mechanical connection between the Chaitenia subduction and that to the north, it is possible that the onset of the Chaitenia SDDS may have contributed to sustaining, if not driving, the protracted Chanic orogeny north of Patagonia. Although this hypothesis provides an elegant explanation for the required trench advance to drive back-arc closure of the Cuyano proto-ocean basin, it warrants further investigation in light of more precise information on the nature and configuration of plate margins during the early Palaeozoic era.

The case of double subduction-induced orogeny in Japan illustrates how subduction interactions, linked to the emergence of a nearby subduction zone, can trigger far-field effects that cascade onto neighbouring plate margins. This perspective offers valuable insight into the interpretation of the seismotectonic setting of northeast Japan, a region renowned for its devastating seismic events, including the Tohoku megathrust earthquake (2011,  $M_w = 9.0$ )<sup>35</sup> and the recent Noto Peninsula intraplate earthquake (2024,  $M_w = 7.6$ )<sup>33</sup> in the back-arc area. With this understanding of the tectonic impact of SDDS zones, we anticipate that a more thorough examination of ancient plate margin geological records will uncover additional cases of double subduction zone-induced orogeny.

## Online content

Any methods, additional references, Nature Portfolio reporting summaries, source data, extended data, supplementary information, acknowledgements, peer review information; details of author contributions and competing interests; and statements of data and code availability are available at <https://doi.org/10.1038/s41561-025-01704-5>.

## References

- Stern, R. J. Subduction zones. *Rev. Geophys.* **40**, 3-1–3-38 (2002).
- Holt, A., Royden, L. & Becker, T. The dynamics of double slab subduction. *Geophys. J. Int.* **209**, 250–265 (2017).
- Pusok, A. E. & Stegman, D. R. Formation and stability of same-dip double subduction systems. *J. Geophys. Res. Solid Earth* **124**, 7387–7412 (2019).
- Király, Á., Holt, A. F., Funiciello, F., Faccenna, C. & Capitanio, F. A. Modeling slab–slab interactions: dynamics of outward dipping double-sided subduction systems. *Geochem. Geophys. Geosyst.* **19**, 693–714 (2018).
- Faccenna, C., Holt, A. F., Becker, T. W., Lallemand, S. & Royden, L. H. Dynamics of the Ryukyu/Izu–Bonin–Marianas double subduction system. *Tectonophysics* **746**, 229–238 (2018).
- Jagoutz, O., Royden, L., Holt, A. F. & Becker, T. W. Anomalously fast convergence of India and Eurasia caused by double subduction. *Nat. Geosci.* **8**, 475–478 (2015).
- Mishin, Y. A., Gerya, T. V., Burg, J.-P. & Connolly, J. A. Dynamics of double subduction: numerical modeling. *Phys. Earth Planet. Inter.* **171**, 280–295 (2008).
- Zhang, K., Liao, J. & Gerya, T. Onset of double subduction controls plate motion reorganisation. *Nat. Comm.* **15**, 1513 (2024).
- Zhang, Q., Guo, F., Zhao, L. & Wu, Y. Geodynamics of divergent double subduction: 3-D numerical modeling of a Cenozoic example in the Molucca Sea region, Indonesia. *J. Geophys. Res. Solid Earth* **122**, 3977–3998 (2017).
- Soesoo, A., Bons, P. D., Gray, D. R. & Foster, D. A. Divergent double subduction: tectonic and petrologic consequences. *Geology* **25**, 755–758 (1997).
- Pindell, J. L. et al. A plate-kinematic framework for models of Caribbean evolution. *Tectonophysics* **155**, 121–138 (1988).
- Santosh, M. A synopsis of recent conceptual models on supercontinent tectonics in relation to mantle dynamics, life evolution and surface environment. *J. Geodyn.* **50**, 116–133 (2010).
- Čížková, H. & Bina, C. R. Geodynamics of trench advance: insights from a Philippine-Sea-style geometry. *Earth Planet. Sci. Lett.* **430**, 408–415 (2015).
- Gürer, D., Granot, R. & van Hinsbergen, D. J. Plate tectonic chain reaction revealed by noise in the Cretaceous quiet zone. *Nat. Geosci.* **15**, 233–239 (2022).
- Jian, H. et al. Slab pull drives IBM trench advance despite the weakened Philippine Sea plate. *Geophys. Res. Lett.* **50**, e2023GL106554 (2023).
- Dewey, J. F. in *The Continental Crust and its Mineral Deposits* Special Paper 20 (ed. Strangway, D. W.) 553–573 (Geological Association of Canada, 1980).
- Sato, H. The relationship between late Cenozoic tectonic events and stress field and basin development in northeast Japan. *J. Geophys. Res. Solid Earth* **99**, 22261–22274 (1994).
- Jolivet, L., Tamaki, K. & Fournier, M. Japan Sea, opening history and mechanism: a synthesis. *J. Geophys. Res. Solid Earth* **99**, 22237–22259 (1994).
- Lallemand, S. & Jolivet, L. Japan Sea: a pull-apart basin? *Earth Planet. Sci. Lett.* **76**, 375–389 (1986).
- Taira, A. Tectonic evolution of the Japanese island arc system. *Ann Rev Earth Planet Sci* **29**, 109–134 (2001).
- Kano, K., Uto, K. & Ohguchi, T. Stratigraphic review of Eocene to Oligocene successions along the eastern Japan Sea: implication for early opening of the Japan Sea. *J. Asian Earth Sci.* **30**, 20–32 (2007).
- Kimura, G. & Tamaki, K. Collision, rotation, and back-arc spreading in the region of the Okhotsk and Japan Seas. *Tectonics* **5**, 389–401 (1986).
- Tamaki, K. Geological structure of the Japan Sea and its tectonic implications. *Chishitsu Chosasho Geppo* **39**, 269–365 (1988).
- Ingle, J. J. Subsidence of the Japan Sea: stratigraphic evidence from ODP sites and onshore sections. In *Proc. Ocean Drilling Program, Scientific Results 1197–1218* (1992); [http://www-odp.tamu.edu/publications/127128SR\\_2/VOLUME/CHAPTERS/sr127128\\_76.pdf](http://www-odp.tamu.edu/publications/127128SR_2/VOLUME/CHAPTERS/sr127128_76.pdf)
- Okada, S. & Ikeda, Y. Quantifying crustal extension and shortening in the back-arc region of northeast Japan. *J. Geophys. Res. Solid Earth* **117**, B01404 (2012).
- Regalla, C., Fisher, D. & Kirby, E. Timing and magnitude of shortening within the inner fore arc of the Japan trench. *J. Geophys. Res. Solid Earth* **115**, B03411 (2010).
- Tamaki, K. & Honza, E. Incipient subduction and deduction along the eastern margin of the Japan Sea. *Tectonophysics* **119**, 381–406 (1985).
- Kim, G.-B., Yoon, S.-H., Kim, S.-S. & So, B.-D. Transition from buckling to subduction on strike-slip continental margins: evidence from the East Sea (Japan Sea). *Geology* **46**, 603–606 (2018).
- Iwasaki, T. et al. Extensional structure in northern Honshu Arc as inferred from seismic refraction/wide-angle reflection profiling. *Geophys. Res. Lett.* **28**, 2329–2332 (2001).
- Wei, D. & Seno, T. in *Mantle Dynamics and Plate Interactions in East Asia Geodynamics Series Vol. 27* (eds Flower, M. F. J. et al.) 337–346 (AGU, 1998).
- Naramura, K. Possible nascent trench along the eastern Japan Sea as the convergent boundary between Eurasian and North American plates. *Bull. Earthq. Res. Inst.* **58**, 711–722 (1983).
- van der Werff, W. Backarc deformation along the eastern Japan Sea margin, offshore northern Honshu. *J. Asian Earth Sci.* **18**, 71–95 (2000).
- Fujii, Y. & Satake, K. Slip distribution of the 2024 Noto Peninsula earthquake ( $M_{JMA} 7.6$ ) estimated from tsunami waveforms and GNSS data. *Earth Planets Space* **76**, 44 (2024).

34. Mazzotti, S., Henry, P. & Le Pichon, X. Transient and permanent deformation of central Japan estimated by GPS: 2. Strain partitioning and arc–arc collision. *Earth Planet. Sci. Lett.* **184**, 455–469 (2001).
35. Ikeda, Y. Strain buildup in the northeast Japan orogen with implications for gigantic subduction earthquakes. *Episodes J. Int. Geosci.* **37**, 234–245 (2014).
36. Pollitz, F. F. Pliocene change in Pacific-plate motion. *Nature* **320**, 738–741 (1986).
37. Lallemand, S., Heuret, A. & Boutelier, D. On the relationships between slab dip, back-arc stress, upper plate absolute motion, and crustal nature in subduction zones. *Geochim. Geophys. Geosyst.* **6**, Q09006 (2005).
38. Schellart, W. P. Overriding plate shortening and extension above subduction zones: a parametric study to explain formation of the Andes mountains. *Geol. Soc. Am. Bull.* **120**, 1441–1454 (2008).
39. Müller, R. D. et al. A global plate model including lithospheric deformation along major rifts and orogens since the Triassic. *Tectonics* **38**, 1884–1907 (2019).
40. Becker, T. W., Schaeffer, A. J., Lebedev, S. & Conrad, C. P. Toward a generalized plate motion reference frame. *Geophys. Res. Lett.* <https://doi.org/10.1002/2015GL063695> (2015).
41. O’Neill, C., Müller, D. & Steinberger, B. On the uncertainties in hot spot reconstructions and the significance of moving hot spot reference frames. *Geochem. Geophys. Geosyst.* **6**, Q04003 (2005).
42. DeMets, C., Gordon, R. G., Argus, D. F. & Stein, S. Effect of recent revisions to the geomagnetic reversal time scale on estimates of current plate motions. *Geophys. Res. Lett.* **21**, 2191–2194 (1994).
43. Gripp, A. E. & Gordon, R. G. Young tracks of hotspots and current plate velocities. *Geophys. J. Int.* **150**, 321–361 (2002).
44. Wu, J., Suppe, J., Lu, R. & Kanda, R. Philippine Sea and East Asian plate tectonics since 52 Ma constrained by new subducted slab reconstruction methods. *J. Geophys. Res. Solid Earth* **121**, 4670–4741 (2016).
45. Takahashi, M. The cause of the east–west contraction of northeast Japan. *J. Geol. Soc. Jpn* **68**, 155–161 (2017).
46. Deschamps, A. & Lallemand, S. The West Philippine Basin: an Eocene to early Oligocene back arc basin opened between two opposed subduction zones. *J. Geophys. Res. Solid Earth* **107**, EPM1-1–EPM1-24 (2002).
47. Ficini, E., Cuffaro, M., Doglioni, C. & Gerya, T. Variable plate kinematics promotes changes in back-arc deformation regime along the north-eastern Eurasia plate boundary. *Sci. Rep.* **14**, 7220 (2024).
48. Heuret, A. & Lallemand, S. Plate motions, slab dynamics and back-arc deformation. *Phys. Earth Plan. Int.* <https://doi.org/10.1016/j.pepi.2004.08.022> (2005).
49. Carlson, R. & Mortera-Gutiérrez, C. Subduction hinge migration along the Izu–Bonin–Mariana arc. *Tectonophysics* **181**, 331–344 (1990).
50. Faccenna, C., Di Giuseppe, E., Funiciello, F., Lallemand, S. & van Hunen, J. Control of seafloor aging on the migration of the Izu–Bonin–Mariana trench. *Earth Planet. Sci. Lett.* **288**, 386–398 (2009).
51. Moreno, E. et al. Numerical modeling of subduction and evaluation of Philippine Sea plate tectonic history along the Nankai trough. *Sci. Rep.* **13**, 18313 (2023).
52. Holt, A. F., Royden, L. H., Becker, T. W. & Faccenna, C. Slab interactions in 3-D subduction settings: the Philippine Sea plate region. *Earth Planet. Sci. Lett.* **489**, 72–83 (2018).
53. Bangerth, W. et al. Geodynamics/ASPECT: ASPECT 2.5.0. Zenodo <https://doi.org/10.5281/zenodo.8200213> (2023).
54. Bangerth, W. et al. ASPECT: Advanced Solver for Planetary Evolution, Convection, and Tectonics, user manual. *figshare* <https://doi.org/10.6084/m9.figshare.4865333> (2023).
55. Kronbichler, M., Heister, T. & Bangerth, W. High accuracy mantle convection simulation through modern numerical methods. *Geophys. J. Int.* **191**, 12–29 (2012).
56. Heister, T., Dannberg, J., Gassmöller, R. & Bangerth, W. High accuracy mantle convection simulation through modern numerical methods-II: realistic models and problems. *Geophys. J. Int.* **210**, 833–851 (2017).
57. Hayes, G. P. et al. Zone geometry model. *Science* **362**, 58–61 (2018).
58. Zhao, D., Wang, J., Huang, Z. & Liu, X. Seismic structure and subduction dynamics of the western Japan arc. *Tectonophysics* <https://doi.org/10.1016/j.tecto.2021.228743> (2021).
59. Auer, L., Boschi, L., Becker, T., Nissen-Meyer, T. & Giardini, D. Savani: a variable resolution whole-mantle model of anisotropic shear velocity variations based on multiple data sets. *J. Geophys. Res. Solid Earth* **119**, 3006–3034 (2014).
60. Funiciello, F. et al. Trench migration, net rotation and slab–mantle coupling. *Earth Planet. Sci. Lett.* **271**, 233–240 (2008).
61. Moresi, L. & Gurnis, M. Constraints on the lateral strength of slabs from three-dimensional dynamic flow models. *Earth Planet. Sci. Lett.* **138**, 15–28 (1996).
62. Mao, W. & Zhong, S. Constraints on mantle viscosity from intermediate-wavelength geoid anomalies in mantle convection models with plate motion history. *J. Geophys. Res. Solid Earth* **126**, e2020JB021561 (2021).
63. Wu, B., Conrad, C. P., Heuret, A., Lithgow-Bertelloni, C. & Lallemand, S. Reconciling strong slab pull and weak plate bending: the plate motion constraint on the strength of mantle slabs. *Earth Planet. Sci. Lett.* **272**, 412–421 (2008).
64. Behr, W. M. & Becker, T. W. Sediment control on subduction plate speeds. *Earth Planet. Sci. Lett.* **502**, 166–173 (2018).
65. Abila, A. L., Behr, W. M. & Ruh, J. Strength of viscous subduction interfaces: a global compilation. *Geology* <https://doi.org/10.1130/G52518.1> (2024).
66. Faccenna, C., Oncken, O., Holt, A. F. & Becker, T. W. Initiation of the Andean orogeny by lower mantle subduction. *Earth Planet. Sci. Lett.* **463**, 189–201 (2017).
67. Capitanio, F. A., Stegman, D. R., Moresi, L. N. & Sharples, W. Upper plate controls on deep subduction, trench migrations and deformations at convergent margins. *Tectonophysics* <https://doi.org/10.1016/j.tecto.2009.08.020> (2010).
68. Holt, A., Becker, T. & Buffett, B. Trench migration and overriding plate stress in dynamic subduction models. *Geophys. J. Int.* <https://doi.org/10.1093/gji/ggv011> (2015).
69. Bogomolov, L., Sim, L. & Kamenev, P. In *Neotectonics and Stressed State Patterns of the Sakhalin Island* (eds Lwisa, E. & Arman, H.) Chap. 3 (IntechOpen, 2020).
70. Hao, M., Li, Y. & Zhuang, W. Crustal movement and strain distribution in East Asia revealed by GPS observations. *Sci. Rep.* **9**, 16797 (2019).
71. Jolivet, L. et al. Neo-Tethys geodynamics and mantle convection: from extension to compression in Africa and a conceptual model for obduction. *Can. J. Earth Sci.* **53**, 1190–1204 (2016).
72. van Hinsbergen, D. J. et al. A record of plume-induced plate rotation triggering subduction initiation. *Nat. Geosci.* **14**, 626–630 (2021).
73. Şengör, A. C. & Stock, J. The Ayyubid Orogen: an ophiolite obduction-driven orogen in the Late Cretaceous of the Neo-Tethyan south margin. *Geosc. Can.* **41**, 225–254 (2014).
74. Kley, J. & Voigt, T. Late Cretaceous intraplate thrusting in central Europe: effect of Africa–Iberia–Europe convergence, not Alpine collision. *Geology* **36**, 839–842 (2008).

75. Rapela, C. W. et al. The Devonian accretionary orogen of the North Patagonian Cordillera. *Gondwana Res.* **96**, 1–21 (2021).
76. Willner, A. P. et al. The geodynamics of collision of a microplate (Chilenia) in Devonian times deduced by the pressure–temperature–time evolution within part of a collisional belt (Guarguaraz Complex, W-Argentina). *Contrib. Mineral. Petrol.* **162**, 303–327 (2011).
77. Dahlquist, J. A. et al. A review of Devonian–Carboniferous magmatism in the central region of Argentina, pre-Andean margin of SW Gondwana. *Earth-Sci. Rev.* **221**, 103781 (2021).

**Publisher's note** Springer Nature remains neutral with regard to jurisdictional claims in published maps and institutional affiliations.

**Open Access** This article is licensed under a Creative Commons Attribution 4.0 International License, which permits use, sharing, adaptation, distribution and reproduction in any medium or format, as long as you give appropriate credit to the original author(s) and the source, provide a link to the Creative Commons licence, and indicate if changes were made. The images or other third party material in this article are included in the article's Creative Commons licence, unless indicated otherwise in a credit line to the material. If material is not included in the article's Creative Commons licence and your intended use is not permitted by statutory regulation or exceeds the permitted use, you will need to obtain permission directly from the copyright holder. To view a copy of this licence, visit <http://creativecommons.org/licenses/by/4.0/>.

© The Author(s) 2025

## Methods

### Numerical subduction modelling

Our 3D subduction models were constructed using the ASPECT finite element code (version 2.5.0)<sup>53–56</sup>. ASPECT was used to solve the conservation of momentum (Stokes equation) and mass (continuity equation) for an incompressible viscous fluid (Boussinesq approximation). Our models are purely compositional. That is, we neglect temperature/thermal diffusion and density and viscosity are purely dependent on compositional fields. Our models contain four compositional fields that have distinct material properties: the crust, upper plate (Eurasia) lithosphere, subducting plate (Philippine Sea plate and Pacific plate) lithosphere, and stiffer material placed at the lateral edges of the Pacific and Eurasian plates (for example, see Extended Data Fig. 3a,c). The background material corresponds to the sub-lithospheric mantle and has another set of mechanical properties (see later paragraphs of this section). The lateral plate edges are imposed to be stiffer (higher viscosity) to retard subduction initiation in these locations. Our models are ‘pseudo-instantaneous’ in that we solve for the velocity and stress fields associated with the imposed slab and plate tectonic geometries, as opposed to allowing the structure/slabs to advect for millions of years. In practice, we extract the solution after 10 kyr of model evolution. Given modelled plate velocities of  $\leq 10 \text{ cm yr}^{-1}$ , we do not observe noticeable advection of the mantle/tectonic plates over this duration.

We use ASPECT’s adaptive mesh refinement functionality to highly refine the finite element mesh within the lithospheric plates—including the crustal layer that makes up the plate boundary shear zone—and within other regions containing large viscosity gradients (for example, the upper-to-lower mantle transition). In these regions, we have a maximum resolution corresponding to ~4-km-wide cubic finite elements. The lowest resolution occurs far away from the tectonic plates and corresponds to ~60-km-wide cubic finite elements. This approach results in ~5,500,000 cells unequally distributed throughout the model domains. Simulations were run on the Skylake (SKX) nodes of the Texas Advanced Computing Center’s Stampede3 cluster.

Our subduction models have a Cartesian domain spanning 8,000 km (trench-perpendicular)  $\times$  5,000 km (trench-parallel)  $\times$  1,000 km (depth). There are no external forces or velocities applied to the subduction system and all model boundaries are mechanically free slip. In our single subduction case, we model Pacific subduction beneath a homogeneous Eurasian plate (Fig. 3a). In the double subduction case, we add the Philippine Sea plate and Ryukyu–Nankai subduction, but leave the Pacific plate/slab geometry completely unchanged (Fig. 3b and Extended Data Fig. 6). At the northern edge of the subduction system ( $y = 5,000 \text{ km}$ ), we impose a ‘free’ plate boundary (that is, tectonic plates are not attached to the model boundary; Extended Data Fig. 3a,c). This enables the Pacific plate to have a north–south velocity component in this northerly model region. At the other side of the subduction system ( $y = 0$ ), the plates are ‘fixed’ to the model boundary. This boundary acts as a plane of symmetry, thereby enabling us to model the diamond-shaped Philippine Sea plate as a triangle (Fig. 3a,b and Extended Data Fig. 3).

We constructed the input plate and slab geometries using the Geodynamic World Builder tool<sup>78,79</sup>. We included only the tectonic complexities that are of first-order importance for our proposed mechanism. Our plate boundaries are linear, aside from the protruding cusp of the Pacific trench in northern Japan. This north–south segment is 1,000 km long and at an angle of  $27^\circ$  relative to the 1,600-km-long northern (Kuril–Kamchatka) and southern (Izu–Bonin) Pacific sections (Fig. 1a). In the double subduction case, the Philippine Sea plate was added by including the Ryukyu–Nankai trenches (Fig. 1a). This Philippine Sea plate–Eurasia plate boundary is 1,700 km long and at  $29^\circ$  to the Japan trench. We adopt a constant Pacific slab geometry from north to south, with the base of the slab extending to 625 km depth. Of the 1,700-km-long Philippine Sea plate–Eurasia plate boundary—in the double subduction system—the southern 1,250 km corresponds to deeper Ryukyu subduction (400 km

slab depth) and the northern 450 km corresponds to shallower Nankai subduction (210 km slab depth)<sup>44,57,58</sup>. Detailed slab geometries are displayed in Extended Data Fig. 3 (cross-sections) and Extended Data Fig. 6 (3D visualization). Both the Pacific and Philippine Sea plate slabs have a slab-top radii of curvature of 185 km and, below this curved portion, dips of  $60^\circ$ . To approximate the interaction of the Pacific slabs with the higher-viscosity lower mantle, we linearly reduce the dip to zero as a function of along-slab distance along the deepest 200 km of the slab. We impose lithospheric thicknesses of 90 km and 60 km for the older and younger Pacific and Philippine Sea plates, respectively, and a 60 km thickness for the idealized Eurasian plate. A weak, 10-km-thick crustal layer is placed on top of all plates and along the upper surface of slabs to 70 km depth. This facilitates plate boundary decoupling, thereby enabling us to reproduce the main features of observed plate and trench velocities (for example, refs. 40,43,48; Fig. 1a). To ensure the Philippine Sea plate (and Nankai slab) and Eurasian plate are also decoupled, a ~150-km-long and 50-km-wide weak zone, with the same properties as the background mantle, is placed at the northern edge of the Philippine Sea plate and Nankai slab. This weak zone extends through the entire plate and has two components: an east–west ( $x$ -directed) component that delineates the northern/top edge of the Philippine Sea plate, and a southeast–northwest component that is parallel to the lateral edge of the northwest-dipping Nankai slab (see Extended Data Fig. 6 for a 3D view of the weak zone). The latter is needed to stop the Nankai slab from intersecting/coupling with the overriding Eurasian plate. To check that the specific geometry of this weak zone does not impact first-order model behaviour, we ran an additional double subduction model with a wider weak region in the triple junction region. In this case, weak material fills the entire region (triangle) between the northern edge of the Nankai slab and its projection onto the Japan trench. Neither the stress pattern nor stress magnitudes are significantly affected (Extended Data Fig. 4b,c).

The Pacific and Philippine Sea lithospheric plates have constant densities of  $3,350 \text{ kg m}^{-3}$ ;  $50 \text{ kg m}^{-3}$  denser than the sub-lithospheric mantle. The Eurasian plate and crustal layers are neutrally buoyant with respect to the mantle, with densities of  $3,300 \text{ kg m}^{-3}$ . This is to approximate the lower densities of continental lithosphere and basaltic crust relative to oceanic lithosphere. The lithospheric and crustal layers are isoviscous and the underlying sub-lithospheric mantle has a composite Newtonian and power-law rheology (for example, ref. 80) to mimic the first-order effects of diffusion and dislocation creep, respectively. Lithospheric plates are set to be 500 times more viscous ( $5 \times 10^{22} \text{ Pa s}$ ) than the reference mantle viscosity ( $10^{20} \text{ Pa s}$ ). This is within the 10–1,000 range of slab–mantle viscosity contrasts generally suggested by geoid constraints<sup>61,62</sup>, slab shapes and trench motions<sup>60,81,82</sup>, and plate bending considerations<sup>63,83,84</sup>. We consider isoviscous plates, that is, without plastic yielding, to both simplify our model setups and minimize nonlinearity (and hence speed up model convergence). While this limits lithospheric deformation to diffuse viscous deformation distributed over hundreds to thousands of kilometres, as opposed to more ‘Earth-like’ localized shear zones, it enables us to examine which regions experience high viscous stress and hence would ultimately be prone to yielding. We increase the lithosphere viscosity by an order of magnitude within 1,000-km-wide (trench-perpendicular) edges of the Eurasian and Pacific plates; this is to ensure that subduction does not initiate at the edges. This higher plate edge viscosity causes the stress discontinuities noticeable at  $x = 1,000 \text{ km}$  and  $6,000 \text{ km}$  (Fig. 3e,f). The crustal layer has a viscosity of  $5 \times 10^{19} \text{ Pa s}$ . Considering a deep plate interface temperature of, for example,  $500\text{--}600^\circ\text{C}$ , and strain rate of  $10^{-12} \text{ s}^{-1}$ , this viscosity overlaps with that recorded for blueschists, and resides between that of stronger meta-basalts and weaker metasediments and serpentinite<sup>64,85–88</sup>. It is also within the  $10^{18}\text{--}10^{20} \text{ Pa s}$  range estimated using numerical shear experiments for the global range of exhumed shear zones lithological distributions<sup>65</sup>. However, given that our simplified shear zone implementation (a single isoviscous layer),

the most appropriate effective shear zone viscosity, is uncertain, we therefore test a range of values (Extended Data Fig. 1).

Power-law flow in the sub-lithospheric mantle is included due to its large effect on plate and trench motions (for example, refs. 89,90). Owing to the compositional nature of our models, we neglect the temperature dependence of mantle viscosity, and additionally omit the pressure dependence. The Newtonian viscosity component of the mantle,  $\eta_N$ , is set to  $2 \times 10^{20}$  Pa s. The power-law component,  $\eta_p$ , is calculated following:

$$\eta_p = \eta_N (\dot{\epsilon}/\dot{\epsilon}_T)^{\frac{1-n}{n}} \quad (1)$$

where  $\dot{\epsilon}$  is the square root of the second invariant of the strain rate tensor,  $n$  is the power-law exponent ( $= 3.5$ ) and  $\dot{\epsilon}_T$  is the transition strain rate. Following ref. 90, we set  $\dot{\epsilon}_T = 5 \times 10^{-15}$  s $^{-1}$ . For strain rates at this value,  $\eta_p = \eta_N = 2 \times 10^{20}$  Pa s. The effective model viscosity is then calculated as:

$$\eta_{\text{eff}} = \left( \frac{1}{\eta_N} + \frac{1}{\eta_p} \right)^{-1} \quad (2)$$

which produces the reference mantle viscosity of  $\eta_{\text{eff}} = 10^{20}$  Pa s at  $\dot{\epsilon} = 5 \times 10^{-15}$  s $^{-1}$ . Given that significant uncertainty remains regarding the appropriate creep law parameters (for example, ref. 91), even for the dominant upper mantle mineral olivine, we consider our simplified mantle rheology to be appropriately complex. Beyond 660 km depth, the lower mantle is set to a viscosity of  $5 \times 10^{21}$  Pa s (that is, a factor 50 increase relative to the reference upper mantle viscosity). This follows geoid and slab sinking rate studies that indicate the lower mantle has a higher viscosity than the upper mantle (for example, refs. 92,93).

To verify that the first-order behaviour of our models does not depend on the assigned crustal and lithospheric viscosities, we have run additional models with different values. Relative to the reference crustal viscosity ( $5 \times 10^{19}$  Pa s), we test a lower value of  $10^{19}$  Pa s and higher values of  $2.5 \times 10^{20}$  Pa s and  $10^{20}$  Pa s (Extended Data Fig. 2). Relative to the reference slab–mantle viscosity ratio (500), we test higher and lower values of 2,000 and 125 (Extended Data Fig. 3). For each of these additional parameter tests, we turn off power-law flow (that is, equation (1)) within the sub-lithospheric mantle and instead use a constant (Newtonian) mantle viscosity of  $10^{20}$  Pa s. Removing this complexity does not substantially affect the modelled stress fields (Fig. 3e–g and Extended Data Figs. 2 and 3), but reduces model run times to ~30% of the equivalent power-law models. Overall, increasing the slab–mantle viscosity ratio and/or decreasing the crustal viscosity increases the magnitude of the double subduction-induced stress increase. However, there is always an increase in horizontal compression due to double subduction.

## Data availability

All data needed to evaluate the conclusions in the paper are presented in this manuscript, the Extended Data figures and the online repository containing the model input files. Model input geometries (for example, plate and slab shapes) were constructed using the Geodynamic World Builder, also available via GitHub at <https://github.com/Geodynamic-WorldBuilder/WorldBuilder>. We provide all ASPECT and Geodynamic World Builder input files needed to run the models as a data publication via Zenodo at <https://doi.org/10.5281/zenodo.15090347> (ref. 94).

## Code availability

All models were run using ASPECT version 2.5.0, which is freely available via GitHub at <https://github.com/geodynamics/aspect>.

## References

78. Fraters, M., Thieulot, C., van den Berg, A. & Spakman, W. The Geodynamic World Builder: a solution for complex initial conditions in numerical modeling. *Solid Earth* **10**, 1785–1807 (2019).
79. Fraters, M. The Geodynamic World Builder. Zenodo <https://doi.org/10.5281/zenodo.3900603> (2020).
80. Zhong, S., Gurnis, M. & Moresi, L. Role of faults, nonlinear rheology, and viscosity structure in generating plates from instantaneous mantle flow models. *J. Geophys. Res. Solid Earth* **103**, 15255–15268 (1998).
81. Stegman, D. R., Freeman, J., Schellart, W. P., Moresi, L. & May, D. Influence of trench width on subduction hinge retreat rates in 3-D models of slab rollback. *Geochem. Geophys. Geosyst.* <https://doi.org/10.1029/2005GC001056> (2006).
82. Ribe, N. M. Bending mechanics and mode selection in free subduction: a thin-sheet analysis. *Geophys. J. Int.* <https://doi.org/10.1111/j.1365-246X.2009.04460.x> (2010).
83. Conrad, C. P. & Hager, B. H. Effects of plate bending and fault strength at subduction zones on plate dynamics. *J. Geophys. Res. Solid Earth* <https://doi.org/10.1029/1999jb900149> (1999).
84. Becker, T. W., Faccenna, C., O’Connell, R. J. & Giardini, D. The development of slabs in the upper mantle: insights from numerical and laboratory experiments. *J. Geophys. Res. Solid Earth* **104**, 15207–15226 (1999).
85. Zhang, J. & Green, H. W. Experimental investigation of eclogite rheology and its fabrics at high temperature and pressure. *J. Met. Geol.* **25**, 97–115 (2007).
86. Hilairat, N. et al. High-pressure creep of serpentine, interseismic deformation, and initiation of subduction. *Science* **318**, 1910–1913 (2007).
87. Hirth, G., Teyssier, C. & Dunlap, J. W. An evaluation of quartzite flow laws based on comparisons between experimentally and naturally deformed rocks. *Int. J. Earth Sci.* **90**, 77–87 (2001).
88. Tokle, L., Hufford, L. J., Behr, W. M., Morales, L. F. G. & Madonna, C. Diffusion creep of sodic amphibole-bearing blueschist limited by microboudinage. *J. Geophys. Res. Solid Earth* **128**, e2023JB026848 (2023).
89. Čížková, H. & Bina, C. R. Effects of mantle and subduction-interface rheologies on slab stagnation and trench rollback. *Earth Planet. Sci. Lett.* <https://doi.org/10.1016/j.epsl.2013.08.011> (2013).
90. Holt, A. & Becker, T. The effect of a power-law mantle viscosity on trench retreat rate. *Geophys. J. Int.* <https://doi.org/10.1093/gji/ggw392> (2017).
91. King, S. D. Reconciling laboratory and observational models of mantle rheology in geodynamic modelling. *J. Geodyn.* <https://doi.org/10.1016/j.jog.2016.03.005> (2016).
92. Hager, B. H. Subducted slabs and the geoid: constraints on mantle rheology and flow. *J. Geophys. Res. Solid Earth* **89**, 6003–6015 (1984).
93. Ricard, Y., Richards, M. A., Lithgow-Bertelloni, C. & Le Stunff, Y. A geodynamic model of mantle density heterogeneity. *J. Geophys. Res. Solid Earth* **98**, 21895–21909 (1993).
94. Gianni, G. M., Guo, Z., Holt, A. F. & Faccenna, C. Model input files for: “Non-collisional orogeny in northeast Japan driven by nearby same-dip double subduction”. Zenodo <https://doi.org/10.5281/zenodo.15090347> (2025).

## Acknowledgements

G.M.G. recognizes the support given by the Alexander von Humboldt Foundation through the Humboldt Research Fellowship for experienced researchers, CONICET, and the funding given by the project PICT-2021-GRF-TI-00541. A.F.H. was supported by the National Science Foundation (NSF; EAR-2147997). Computational resources were provided by NSF ACCESS under allocation EAR180026 to A.F.H. We also thank the Computational Infrastructure for Geodynamics ([geodynamics.org](http://geodynamics.org)), which is funded

by NSF EAR-0949446 and NSF EAR-1550901, for supporting the development of ASPECT.

## Author contributions

G.M.G. conceived the study. Z.G. and A.F.H. designed and carried out the numerical modelling. C.F. provided background on the study area and geodynamic processes. All authors contributed to writing and editing the manuscript, as well as creating the figures.

## Funding

Open access funding provided by GFZ Helmholtz-Zentrum für Geoforschung.

## Competing interests

The authors declare no competing interests.

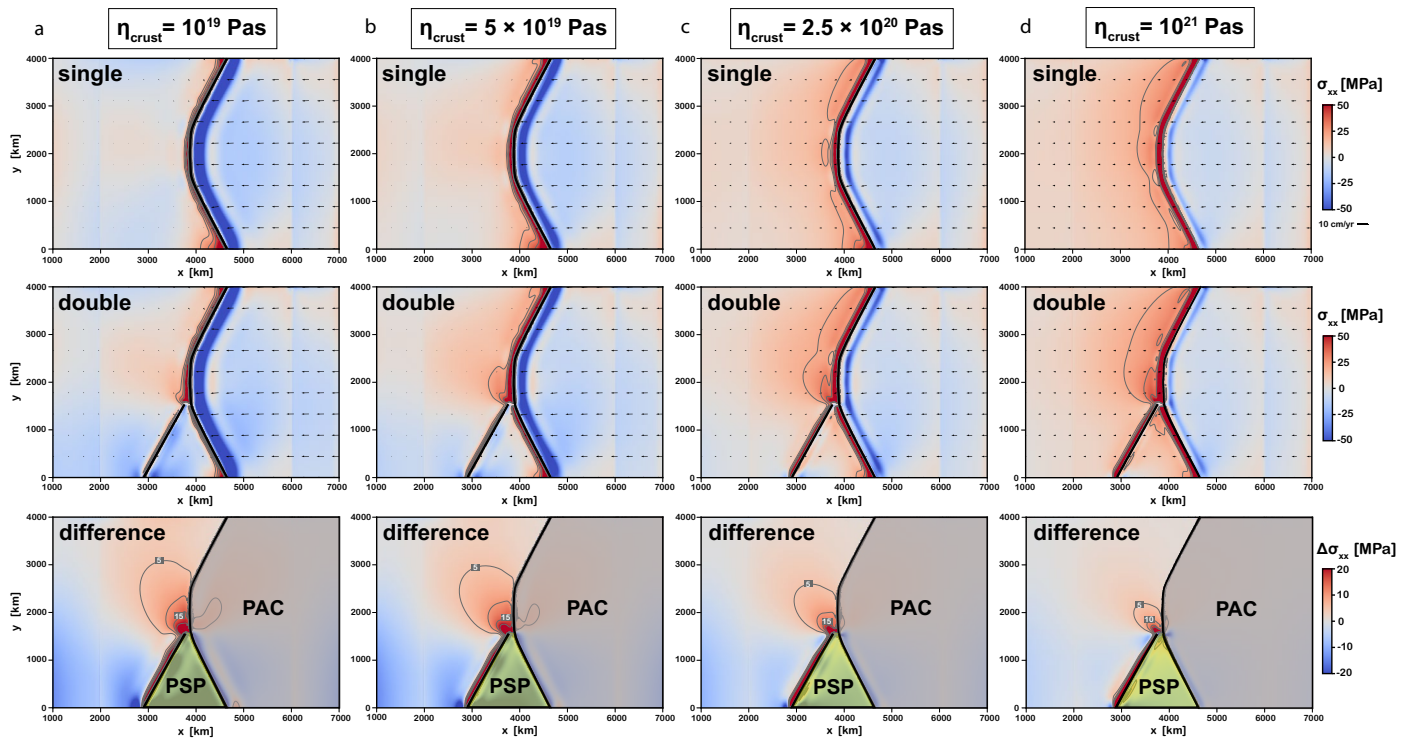
## Additional information

**Extended data** is available for this paper at  
<https://doi.org/10.1038/s41561-025-01704-5>.

**Correspondence and requests for materials** should be addressed to Guido M. Gianni.

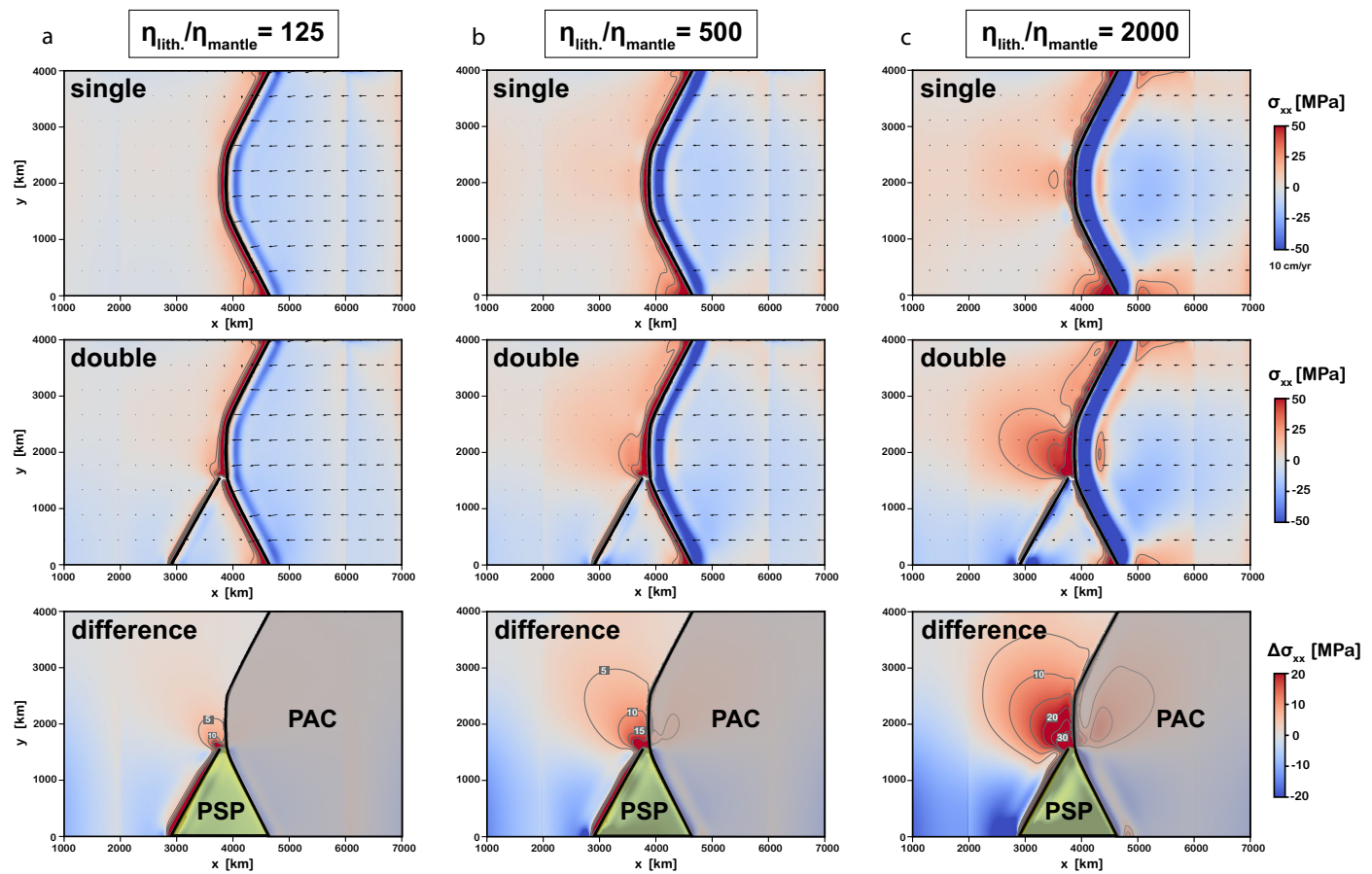
**Peer review information** *Nature Geoscience* thanks Miao Dong, Gaku Kimura and the other, anonymous, reviewer(s) for their contribution to the peer review of this work. Primary Handling Editor: Stefan Lachowycz, in collaboration with the *Nature Geoscience* team.

**Reprints and permissions information** is available at  
[www.nature.com/reprints](http://www.nature.com/reprints).



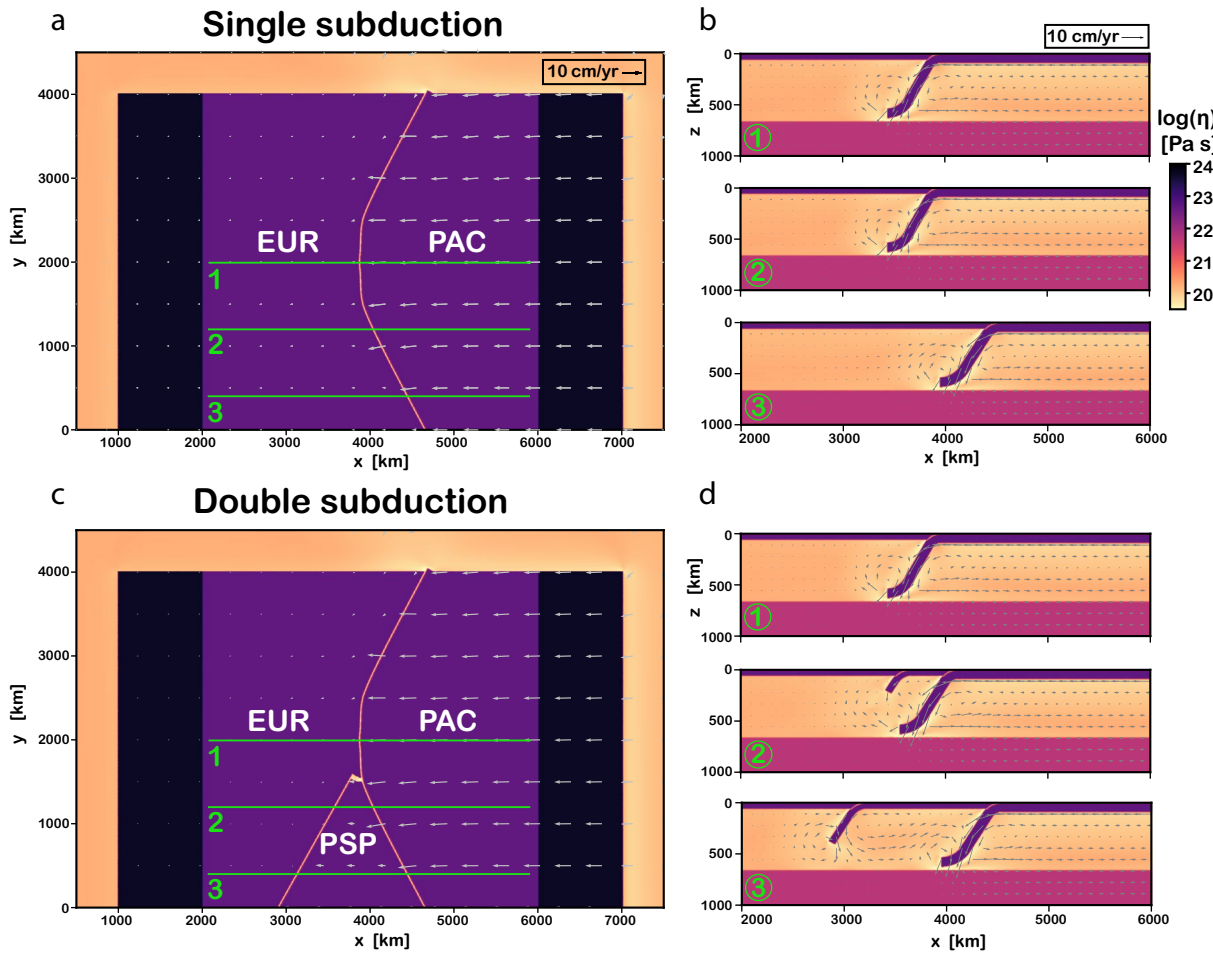
**Extended Data Fig. 1 | The impact of variable crustal viscosity on the horizontal deviatoric normal stress (x-direction) in single slab models, double slab models and the difference between single and double slab cases.** Crust viscosities tested are  $10^{19} \text{ Pas}$  **a**,  $5 \times 10^{19} \text{ Pas}$  **b**,  $2.5 \times 10^{20} \text{ Pas}$  **c**, and  $10^{21} \text{ Pas}$  **d**. All other parameter values are held constant, including the lithosphere-mantle

viscosity ratio of 500. The crust viscosity of panel **b** ( $5 \times 10^{19} \text{ Pas}$ ) is equivalent to that within the reference models presented in the main text. However, unlike in the reference models, the power-law mantle viscosity component is turned off in this suite of models. Abbreviations are: PSP: Philippine Sea Plate and PAC: Pacific Plate.



**Extended Data Fig. 2 | The impact of variable lithosphere/slab viscosities ( $\eta$ ) on the horizontal deviatoric normal stress (x-direction) in single slab models (upper row), double slab models (middle row) and the difference between single and double slab cases (bottom row). The slab-mantle viscosity ratios tested are 125 a, 500 b, and 2000 c. All other parameter values are held constant,**

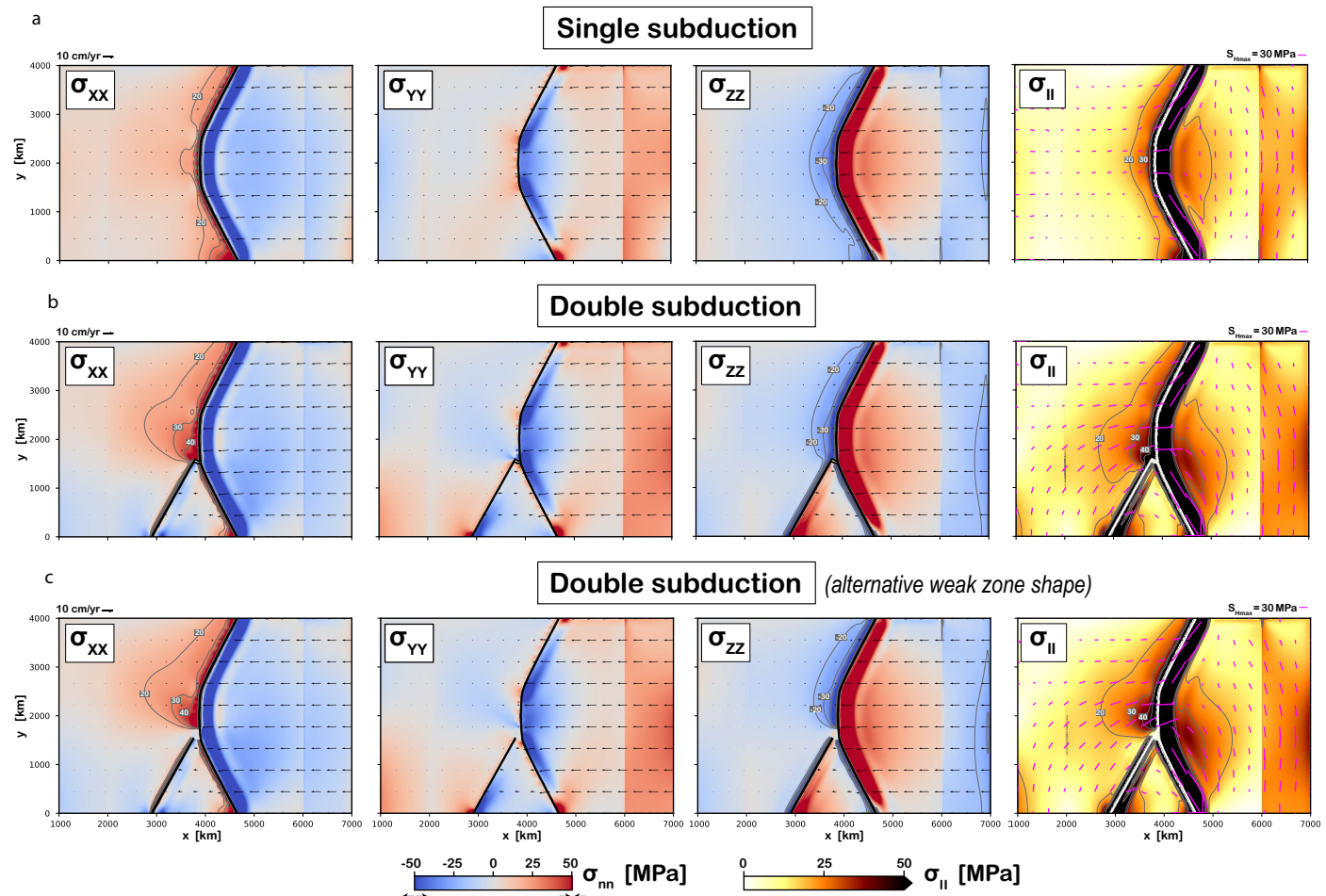
including the crust viscosity of  $5 \times 10^{19}$  Pas. The slab-mantle viscosity ratio of panel b (500) is equivalent to that of the reference models presented in the main text. However, unlike in the reference models, power-law viscosity in the mantle is turned off in these models. Abbreviations are: PSP: Philippine Sea Plate and PAC: Pacific Plate.



**Extended Data Fig. 3 | Viscosity and velocity fields of the reference single and double subduction models (that is, the models presented in the main text).**

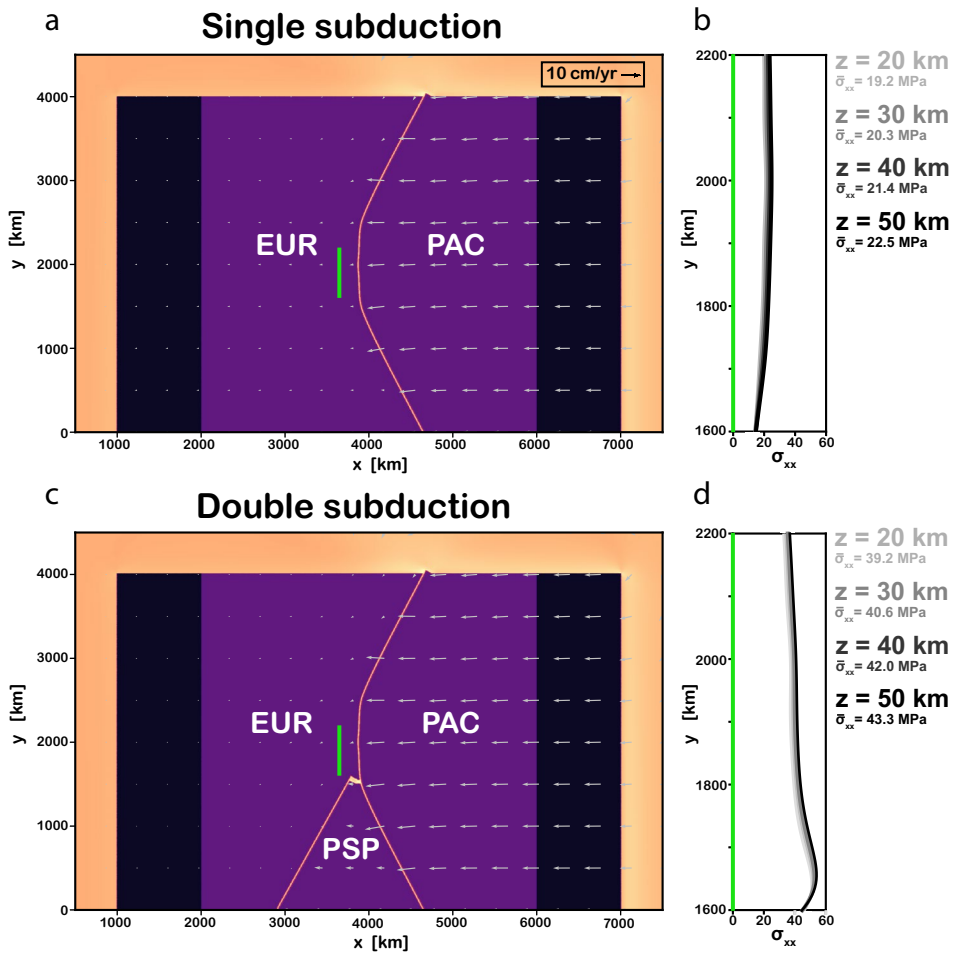
For both models, we present a horizontal slice (panels a, c) and vertical cross sections at equivalent locations along the Pacific trench (b, d). The horizontal slices are at 30 km depth, that is, beneath the weak crust and through the center

of the lithosphere. In the vertical slices, note the localized viscosity reductions adjacent to the slabs due to the power-law component of sub-lithospheric mantle viscosity. Profiles number 1 and 3 are those presented in Fig. 1 in the main text. Abbreviations are: EUR: Eurasian Plate; PSP: Phillipine Sea Plate, and PAC:



**Extended Data Fig. 4 | More detailed lithospheric stress analysis.** This analysis involves: Deviatoric normal stress components, the second invariant of the deviatoric stress (square root), and the maximum horizontal compressive stress axes for: a, the reference single subduction model, b, the reference double

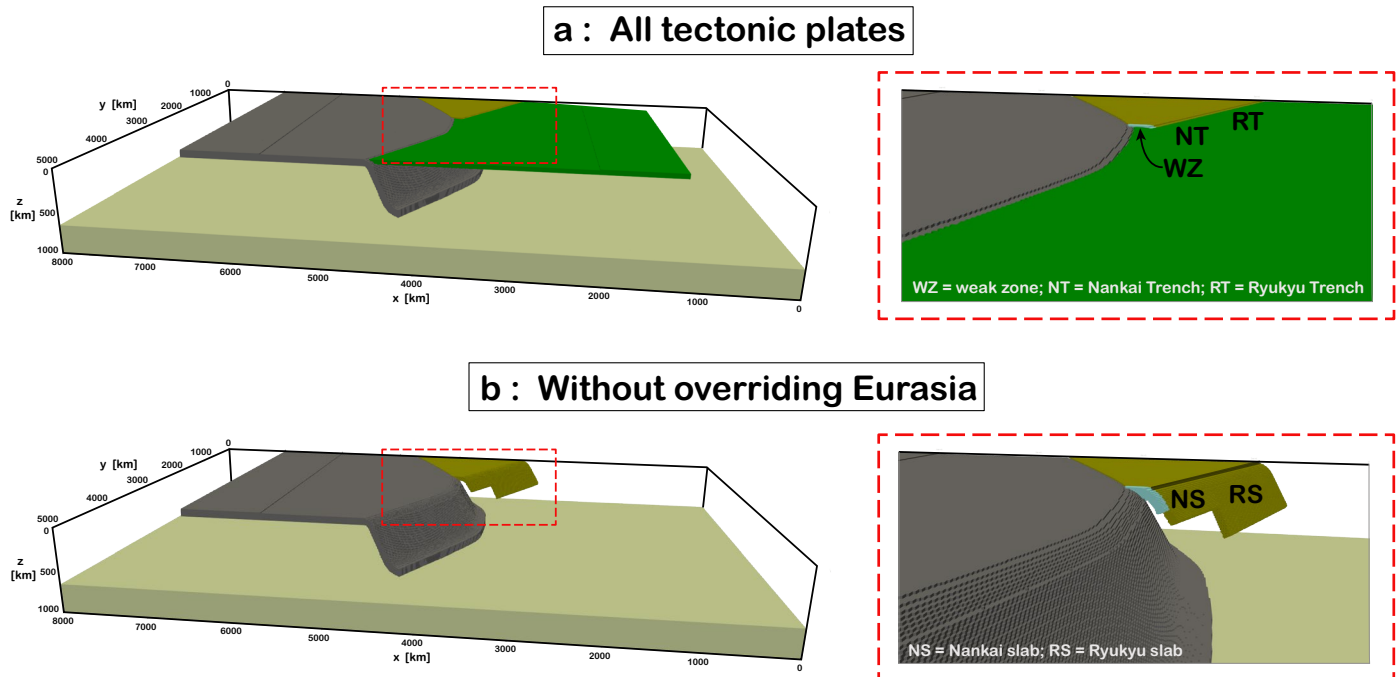
subduction model, and c, a double subduction model with a wider weak zone in the triple junction region. In the weak zone test, the weak material fills the entire region between the edge of the Nankai slab and its projection into the Japan trench.



**Extended Data Fig. 5 | The impact of double subduction on the horizontal normal stress (x-direction) in the Japan region in the reference single and double subduction models (that is, the models presented in the main text).**

For both models- single and double subduction - we present a horizontal slice (panels **a**, **c**) and along strike profiles of the horizontal normal stress at

lithospheric depths from 20 km to 50 km (**b**, **d**). Panels **a** and **c** are equivalent to those of Extended Data Fig. 3 (with the location of the stress profiles marked). We annotate the mean horizontal normal stress (x-direction) of the profiles. At all depths, the introduction of double subduction approximately doubles the compressive stress magnitude.



**Extended Data Fig. 6 | 3-D views of the tectonic geometry imposed within the double subduction models.** The left panels display the entire domain with all tectonic plates (a) and without overriding plates (b) with a view looking from the North/high y-values. The bottom-left panel is modified only in that it does not

include the overriding Eurasia (to display the Nankai-Ryukyu subduction zone). The right panels are zoom-ins around the Philippine Sea Plate (PSP) region. In addition to the lower mantle, all three tectonic plates and all slabs are shown. The weak zone decoupling the PSP and Eurasia is also displayed within the zoom-ins.